

The Numerical Analysis of the Suppression of Flow-Induced Vibrations using Slits at the Laminar Regime

Anas Ghannam ^a, Mohammad Belal ^a and Isam Janajreh ^{a*}

^a Department of Mechanical Engineering, Khalifa University of Science and Technology, P.O. Box 127788, Abu Dhabi, United Arab Emirates

Abstract

The flow over a cylinder is responsible for stimulating vibrations on circular cylinders due to the flow separation and periodic vortex shedding at the downstream area of the cylinder near the wake. Significant damage and fatigue failure transpire when the vortex shedding frequency coincides with the structure's natural frequency, leading to a severe financial and human catastrophe. Therefore, this paper aims to establish a passive control method suppressing the flow induced vibrations (FIVs) by incorporating parallel slits with different sizing examined at various mounting conditions. Using ANSYS, a series of numerical simulations are carried out to a 1-degree-of-freedom system with 10% and 20% width to diameter ratio (W/D) parallel slits in the laminar regime ($Re=100$). The effect of various parameters such as the slit width to diameter ratio (W/D) and the reduced velocity (U_r) to control the oscillating motion of the cylinder is analyzed using normalized oscillation amplitude, root mean square value of lift coefficient, mean drag coefficient, transverse oscillations frequency and vortex shedding patterns. The findings reveal that the passive parallel slit, with a greater width to diameter ratio than 10%, can subdue the cylinder oscillations and reduce drag and lift forces. Furthermore, lock-in phenomena responsible for substantial structural damage are witnessed at 6 to 8 reduced velocities. Finally, remarkable vortex shedding patterns are visualized at a reduced velocity of 4, justifying high amplitude cylinder displacement.

Keywords: Flow induced vibrations, Slits, Laminar, Passive flow control

1. Introduction

The flow across a bluff body is a very occurring phenomenon in real life as they are found in many industrial applications such as shell and tube heat exchangers, cooling towers, and flow over high-rise and offshore structures. The separation point and vortex shedding describe the behavior of a flow across a cylinder. At the separation point, the flow is induced, and vortices are formed. The flow-induced motion from the interactions of the flow and the structural body is described as flow-induced vibrations (FIV) [1]. These vibrations of a flexible structure are critical when the vortex shedding frequency and the structure's natural frequency are equal. Such synchronization is called lock-in or lock-on, which is responsible for diminishing the structural integrity of the cylinders and inducing fatigue [2]. In addition, catastrophic damage is also inflicted on humans and

the environment, with the additional financial costs reaching a range of one million to one billion dollars [3]. On the other hand, oscillating vibrations can be utilized in the energy harvesting of the flow. However, such implementation is not focused on in this work.

In the last decades, various studies have been conducted on FIVs and the critical affecting parameters on the oscillation of cylinders. The literature either focused on studying the operating parameters in flow-induced vibrations on single and tandem cylinders or on distinct technologies to investigate and eliminate FIVs.

Olsen & Rajagopalan [4] have used circular cylinders modified with an axial slit with a concave rear notch to investigate the vortex-shedding phenomenon. The Strouhal number/Reynolds number (St/Re) relationship and the estimation of the drag coefficient (C_D) received special attention. It was found that the relationship for the modified cylinders differed noticeably from

* Corresponding author. Tel.: +971 2 312 3286

Fax: +971 2 312 3286; E-mail: isam.janajreh@ku.ac.ae

© 2016 International Association for Sharing Knowledge and Sustainability

DOI: 10.5383/ijtee.19.02.003

that of a circular cylinder, especially for the cylinder with a slit normal to the flow, where the Strouhal number was consistently greater than for a circular cylinder over the range of Reynolds number of ($60 < Re < 1000$). In comparison to the value of 0.94 for a circular cylinder, the estimated values of (C_D) at Reynolds number 2200 for a cylinder with a slit normal to the flow and for a cylinder with a concave rear surface were 1.41 and 2.52, respectively.

Likewise, Gao et al. [5] have experimentally investigated the Characteristics of flow around a modified circular cylinder. Based on the cylinder diameter D and the incoming airflow speed, the experimental campaign was carried out in a wind tunnel at a Reynolds number of $Re = 2.67$. A slit parallel to the incoming airflow is added to the cylindrical test model to create a channel for flow communication between the windward and leeward stagnation regions. The slit width S increases by $0.025 D$, from $0.05 D$ to $0.15 D$. A particle image velocimetry (PIV) system was used to assess the wake flow patterns of the natural and modified cylindrical test models. Pressure distributions on the cylinder surface were evaluated to estimate the aerodynamic forces operating on the test model. The findings of the experiment show that a slit helps to lower the drag and decrease the varying amplitude of the dynamic wind loads operating on the test model. The PIV measurement findings show clearly that the slit creates a self-issuing jet into the cylinder wake and that the passive jet is efficient in controlling the wake vortex shedding process from the circular cylinder.

In addition, Ali et al. [6] have numerically investigated the oscillating circular cylinder placed in a uniform stream. To simulate particular instances of flow-induced vibrations, the cylinder is driven into transverse oscillations. The frequency ratio can range from 0 to 2, with 0 indicating a stationary cylinder. The findings show that the frequency and amplitude of the lift and drag coefficients are modulated by the cylinder oscillation. When the cylinder oscillation frequency and its natural frequency of vortex shedding are in sync, the lock-in takes place at a frequency ratio of 1. The lock-in situation has the highest average drag coefficient, while the lift coefficient is seen to rise with the frequency ratio. In all of the cases examined, the 2S vortex shedding pattern can be seen in the vorticity contours. On the other hand, Hassan et al. [7] have investigated a flow of low Reynolds number ($Re = 100$) across a slitted, two-dimensional cylinder to explore the flow characteristics within the slit and the impact they have on the shedding frequency. To complete the task, computational techniques were used to try and solve the unstable Navier-Stokes equations. Utilizing the 2D vertical soap film tunnel that is available in our lab at Khalifa University, validation was carried out experimentally. The results show a good agreement between numerical and experimental data.

As mentioned earlier, parameters affecting the behavior of tandem cylinders in induced flow are a trendy topic in the industry. Khan et al. [1] have examined the impact of three tandem cylinders' different diameters on the FIVs and convection heat transfer characteristics. Through numerical experiments, the effects of the diameter reduction ratio on FIVs and the aspects of heat transfer through flow structures, oscillation amplitude, shedding frequency, the relationship between lift coefficient and cylinder displacement, and Nusselt number were all investigated. According to the results, the three tandem cylinders' diameter reduction ratio reduces oscillation amplitude while enhancing heat conduction to the cylinder. As the diameter reduction ratio is raised, the most significant downstream cylinder oscillation amplitude decreases to a smaller Ur . The oscillation amplitude for diameter reduction

ratio = 0.4 is less than for an isolated cylinder and diameter reduction ratio = 0.

Similarly, Zhang et al. [8] have numerically investigated a two-dimensional model of the FIV of two rigidly linked square cylinders arranged in tandem with Reynolds number of 100 and 200 and a gap of $L/D = 2.0$ and 6.0 . First, the flow structures and dynamic response are examined. Based on appropriate orthogonal decomposition, modes-based energy transfer analysis was created. The primary mechanism of the FIV was then discovered by studying the energy transfer between the cylinders and the coherence modes. The findings show that the soft lock-in phenomenon was seen in every instance. The dynamic response is always less than that of a stationary cylinder when the gap $L/D = 2.0$, and all wake structures exhibit "2S" modes due to the upstream cylinder's stabilized effects. One study has also investigated the FIV of two tandem cylinders with different diameters at a Reynolds number of 100 and a range of reduced velocities of 2 to 10 [9]. The impacts of the cylinder diameter ratio (0.2 to 1) and the cylinder spacing ratios 1.5, 3.5, and 5.5 on vibration responses, frequency responses, lock-in, and wake structure are considered in particular. The maximum possible oscillation amplitude is obtained by selecting a mass ratio of the cylinder to the fluid as one and the damping coefficient as zero. The findings show that the wake interference is complex and that FIV is very sensitive to both diameter and spacing ratios. The upstream cylinder oscillation is impacted by a fall in diameter ratio due to a change in its effective Reynolds number. In contrast, the downstream cylinder is significantly impacted by its wake.

Some scholars have performed different techniques to study the FIV's. Sonawane et al. [10] have performed a numerical simulation of an unstable laminar viscous incompressible flow over a cooled circular cylinder that is vibrating due to the flow's induced vibration, both with and without active thermal buoyancy. A novel ALE-HLLC-AC formulation serves as the foundation for the internally designed solver. In ALE formulation for moving boundary problems, the artificial compressibility method is employed for incompressible flow. Gradient computations based on solution-dependent weighted least - square are used to achieve high order accuracy. Reynolds number (Re) = 150, mass ratio = 2, Prandtl number = 7.1, and Richardson number = (-1,0) are used to simulate the flow. The current solver effectively creates VIV flow over a cooled, circular cylinder. The current solver, as discussed, solves the continuity and momentum equations simultaneously, so it is anticipated to be faster. The solution-dependent weighted least square-based gradient calculation can also achieve near quadratic order of accuracy on unstructured data structures, producing high order accurate results. An excellent match between the oscillation amplitude and temperature field of the vibrating cylinder and the result from the literature suggests that the current approach might be utilized to investigate fluid-structure interaction issues like energy harvesters. Moreover, Nguyen & Nguyen [11] have suggested using the detached eddy simulation method for the simulation of incompressible Navier-Stokes flows over cylindrical structures coupled with their rigid body motions. In this method, high Reynolds number flows over free oscillating cylinders are modeled using a hybrid turbulence model based on Reynolds average Navier-Stokes and large eddy simulations, where Reynolds average Navier-Stokes is used to represent near wall flow features and large eddy simulations are used to resolve wake dynamics. The suggested method has been validated in numerous experimental setups with fixed cylinders and cylinders vibrating as a result of vortex induction. A numerical experiment demonstrating the effectiveness of the proposed approach for cylinders with a single degree of freedom (cross-flow oscillations) and two degrees of freedom (in-plane

oscillations) illustrates its capacity to capture fundamental VIV characteristics and predict responses of cylinders with reasonable accuracy for a range of reduced velocities and mass ratios. For the benchmark test cases that are provided, numerical prediction is in good agreement with prior experimental investigations. In addition, Ali et al. [12] have conducted numerical studies on how heat transfer and cylinder rotation affect the induced forces brought on by vortex shedding. The flow is kept at a 100 Reynolds number. A temperature difference between the cylinder wall and the entering flow of between 300K and 900K is utilized. Using Ansys/Fluent, transient analysis is carried out to solve Unsteady Reynolds Averaged-Navier-Stokes (URANS). A user-defined function causes the cylinder to rotate oscillatory in both the clockwise and counterclockwise directions. It is discovered that the drag and lift coefficients' amplitude and frequency are dampened by heat transfer. In contrast, the oscillatory rotation of the cylinder causes their amplitude to be modulated and causes a rise in the drag and lift coefficients, particularly during the lock-on condition.

As studies investigated crucial parameters, others focused on limiting FIVs. Methods to eliminate FIVs are divided into active and passive techniques. The active method controls the oscillations by an external power input. However, the passive control utilizes geometry modifications to suppress the flow. Because active methods require continuous maintenance and additional costs, the literature focuses more on passive controlling methods. One of which is Su et al. [13] study which proposed to suppress or enhance the FIVs of a circular cylinder by placing a small-size square plate in its wake. Due to the square plate's separation from the circular cylinder, it interferes with the wake flow and alters the circular cylinder's FIV. When compared to alternative modification methods that span the whole length of the circular cylinder, the additional cost of the modification can be significantly reduced because the square plate is only present at a single (and frequently short) segment of the cylinder. To demonstrate the effectiveness of the downstream square plate and examine the effects of various factors, several wind tunnel tests are conducted (e.g., plate size and position). According to experimental findings, the size of the plate, the space between it and the cylinder, and the lateral distance all have a major impact on the downstream square plate's impact.

Furthermore, Hsu & Chen [14] have simulated flow along a cylinder with a straight or inclined slit using the spectral element approach for Reynolds numbers between 100 and 500. With the exception of low Reynolds numbers, such as $Re=100$, the drag rises as the slit's angle of inclination increases and is more than that for a cylinder without a slit for flow in the blowing/suction mode. The frequency of vortex shedding rises when the angle of inclination is increased. However, the greater angle of inclination also increases drag. Moreover, the aerodynamic forces brought on by pressure or shear stress on the exterior surface and the slit change with the slit's angle of inclination. Moreover, Ali et al. [15] have numerically and experimentally examined the flow over a slit (0.1D) cylinder at $Re = 100$ at various slit angles ($0^\circ - 90^\circ$) using CFD and soap-film. The URANS equations are solved to yield the numerical solution, and the coefficients of lift (C_L) and drag (C_D), velocity, and vorticity are examined. Experimentally, soap film is utilized to visually validate the flow pattern scaler data. According to the findings, passive slit has a minor impact on the C_L and average C_D but has no noticeable impact on the overall flow pattern. Actively altering the wall oscillation's amplitude and frequency, however, has a greater impact. The average C_D only increased at the lock-in condition and slightly decreased at the other

frequencies; however, the C_L amplitude increases with increasing frequency of wall oscillation.

Furthermore, Mishra & De [16] have explored the suppression of VIVs in the laminar domain ($Re = 100-500$) using a passive flow control technique (slit through a circular cylinder). The root mean square value of the lift coefficient decreases with S/D up to $Re 300$, which in turn suppresses vortex shedding. The form of vortex shedding stays periodic for all S/D. When $Re > 300$, the lift coefficient's root mean square value drops up to S/D 0.15 and the flow exhibits periodic vortex shedding; however, once $S/D > 0.15$, the flow exhibits irregular vortex shedding downstream of the cylinder, causing the root mean square to increase. The bifurcation points where the flow changes its behavior from a symmetric to an asymmetric solution at $Re=232$ and then back to a symmetric solution at $Re=304$ are visible in the variation of the Re for the $S/D = 0.20$. The investigation of the unsteady flow through the modified cylinder further shows that the vortex shedding is suppressed; The analysis does offer the qualitative property of suppression, though. Quantifying suppression and examining the dominant vortical structure for the slit through the cylinder are done using reduced-order models, specifically Proper Orthogonal Decomposition and Dynamic Mode Decomposition.

As researchers proposed various methods to suppress FIVs, few have experimented with the effect of passive horizontal slits at different slit widths on FIVs in a laminar regime in selected reduced velocities. The novel concept of abstaining from the oscillations of the cylinder might have the potential to eliminate the current dilemma. This study aims to compare the drag coefficient, the lift coefficient, and oscillating amplitude for the slitted cylinder at slit width-to-diameter percentages of 10% and 20% at different reduced velocities (U_r).

The paper's organization is as follows: Section 2 presents the mathematical model used in this analysis. In addition, the study aims to develop a mesh sensitivity analysis for the numerical model to acquire fidelity of the work. Afterward, the study is validated with the literature to ensure adequate inputs of the model. Finally, section 3 reports the detailed findings of the effect of the slits with different slit sizes on the oscillating amplitude, drag coefficient, and lift coefficient across various reduced velocities, followed by the conclusion and outlook in Section 4.

2. Methodology

2.1. Problem description

This paper investigates slits with 10% and 20% width-to-diameter ratios (W/D) in an oscillating cylinder to suppress flow-induced vibrations (FIVs) at $Re = 100$. The induced fluid is air and considered steady, newtonian, incompressible, and a d laminar two-dimensional flow. To avoid implementing additional boundary conditions, in the case of rectangular domain, the study is utilizing a circular domain. The circular domain reduces the blockage ratio significantly compared to the rectangular domain. The domain consists of two coinciding circles; the outer cylinder with a diameter of 64 times the inner solid cylinder to capture the vortex shedding and oscillation fully. The moving mesh is inflated until 16 times the diameter of the solid cylinder. It uses a remeshing technique which dissimilar to sliding mesh implemented elsewhere [17]. Figure 1 demonstrates the model's domain of the study along with the boundary conditions.

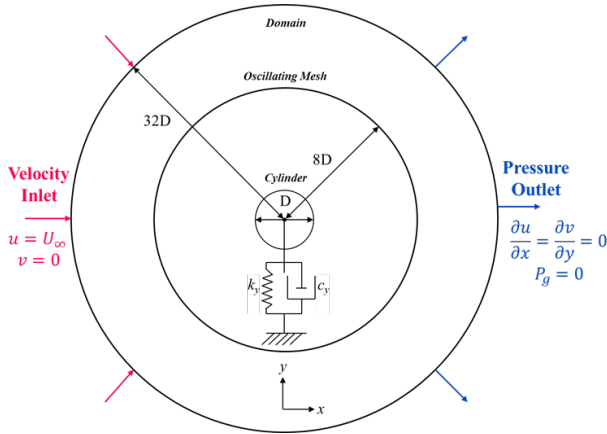


Fig. 1: Illustration of the computational domain (not to scale).

2.2. Governing equations

The numerical approach of the study is a transient incompressible laminar flow over a cylinder. Body forces are neglected in this study assuming a planer flow. Therefore, the continuity, and momentum equations of this study in indicial form are written per Eq. 1 and Eq. 2 as:

$$\frac{\partial u_i}{\partial x_i} = 0 \quad (1)$$

$$\frac{\partial u_i}{\partial t} + \frac{\partial u_i u_j}{\partial x_j} = -\frac{\partial P}{\partial x_i} + \frac{1}{Re} \left[\frac{\partial^2 u_i}{\partial x_j \partial x_j} \right] \quad (2)$$

Where u , P , and Re are the velocity, pressure, and Reynolds number given as $Re = \frac{\rho U_\infty D}{\nu}$ with U_∞ here is the far stream velocity and D is the diameter of the solid cylinder. The thermophysical properties of the fluid are the density (ρ) and kinematic viscosity (ν). The i and j are the indices of the vectors ranging from 1 to 3. The cylinder is oscillating in the transverse direction and prescribed by the 2nd order mass-dashpot-spring Eq. 3 as:

$$m\ddot{y} + c\dot{y} + ky = F_L \quad (3)$$

Where \ddot{y} , \dot{y} , and y are the acceleration, velocity and displacement in the transvers y -direction, respectively. The m is the virtual mass of the system, c is the damping coefficient, k is the spring constant and F_L is the lift force. Eq. 3 could be simplified as:

$$\ddot{y} + 2\zeta\omega_n\dot{y} + (k/m)y = F_L/m \quad (4)$$

Where ζ is the damping ratio defined as the ratio between damping coefficient c and $2\sqrt{km}$. The ω_n is the angular natural frequency in rad/s defined as:

$$\omega_n = 2\pi f_n = \sqrt{k/m} \quad (5)$$

Where f_n is the natural frequency of the system. Finally, Eq. 4 is modified to the non-dimensional form as:

$$\ddot{Y} + \frac{4\pi\zeta}{U_r}\dot{Y} + \left(\frac{2\pi}{U_r}\right)^2 Y = \frac{C_L}{2m^*} \quad (6)$$

In which \ddot{Y} , \dot{Y} , and Y are the non-dimensional acceleration, velocity, and displacement in y direction, respectively. The U_r , C_L and m^* are the reduced velocity, lift coefficient, and mass ratio, respectively. In this work, the nondimensional natural frequency is defined as:

$$f_n = 1/U_r \quad (7)$$

Where it varies depending on the reduced velocity, the reduced is a crucial parameter in this study where it controls the behavior of the elastically mounted cylinder and is used as a unifying parameter that regulates the coefficients in the equation of the system. The mass ratio is attained by dividing the mass of the cylinder by the mass of the displaced fluid given by:

$$m_f = \rho\pi D^2 l/4 \quad (8)$$

In which ρ is the density of the fluid and l is the depth considered as unit length. Finally, the lift coefficient (C_L), drag coefficient (C_D) and excitation frequency (f_{ex}) are given as:

$$C_L = \frac{2F_L}{\rho D U_\infty^2} \quad (9)$$

$$C_D = \frac{2F_D}{\rho D U_\infty^2} \quad (10)$$

$$f_{ex} = \frac{1}{2\pi} \sqrt{\frac{k}{m+\Delta m}} \quad (11)$$

Where U_∞ is the free stream velocity, Δm is the added mass.

2.3 Boundary conditions

The system consists of one degree of freedom that oscillates in the transverse direction. Dirichlet boundary conditions are applied on the upstream/left-side of the domain with velocity in the longitudinal direction resulting in a Reynolds number of 100. The other side of the domain is given as the Neumann boundary condition with zero-gauge pressure. No slip and penetration conditions are applied on the solid cylinder wall. The mass ratio m^* defined as the ratio between the mass of the cylinder and the mass of the displaced fluid, is selected as 1.88. The reason behind such a decision is to compare the model's solid cylinder with the literature and subsequently assess the findings of the slit cylinder. Similarly, the study uses a damping ratio $\zeta = 5.42 \times 10^{-3}$. The spring constant and natural frequency are attained from the range of reduced velocities. The range of reduced velocities tested in this study is 2, 4, 6, 8 and 10.

2.4 Computational model

ANSYS Gambit is utilized to build a structured quadrilateral mesh grid with minimum sizing at the cylinder surface and with inflating in size near 1.2 when moving away from the surface of the cylinder. Figure 2 represents the fine mesh for slitted cylinder used in the study. The mesh is divided into two divisions; the outer ring represents the static mesh, and the inner circle represents the oscillating mesh. The oscillating mesh, also called the dynamic mesh. It is unsteady transverse motion is controlled via a user-defined function (UDF). In the UDF file, the equation of motion is manipulated to test the effect of various reduced velocities. The governing equations are solved by the 2nd order upwind method selected in the software with the residuals set to $10e^{-6}$ for the convergence in the governing equations. In the unsteady analysis, the dimensionless time step plays a significant role. Therefore, Courant–Friedrichs–Lewy (CFL) number is monitored throughout the selection of the time step to ensure it remains below 1 for physical stability.

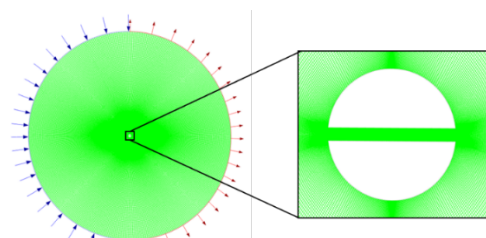


Fig. 2: The discretized mesh for a 10% slitted cylinder.

2.5 Mesh independence study and model validation

The constructed mesh robustness and accuracy is assessed by generating four different mesh sizes (fine, baseline, coarse I, and coarse II) and reporting the Strouhal number for each. As illustrated in Table 1, the relative errors based on the fine mesh were 1.164 for the baseline compared to 1.32 and 1.482 for the coarse I and coarse II meshes, respectively. This asserts the appropriateness of the baseline mesh and subsequently is used as compromise between computational cost/power and accuracy.

Table 1 The mesh sensitivity analysis on various mesh sizes

Type of Mesh	Number of elements	Strouhal number	Error percentage (%)
Fine	73,000	0.16667	---
Baseline	36,000	0.16473	1.164
Coarse I	18,000	0.16447	1.320
Coarse II	9,000	0.16420	1.482

Furthermore, to insure of the accuracy of the numerical model, a comparison of the findings with the literature is done. The study evaluates the nondimensional displacement amplitude of the cylinder (A_y/D) and its structure vibrational frequency (f_s/f_n) with those reported elsewhere [18] [19]. It should be noted that the literature work carried out at $Re=100$, $m^* = 1.88$ and $\zeta = 5.42 \times 10^{-3}$. Figures 3 and 4 overlays the current and literature results. The graphs indicate that a good agreement between the current baseline model and the reported literature.

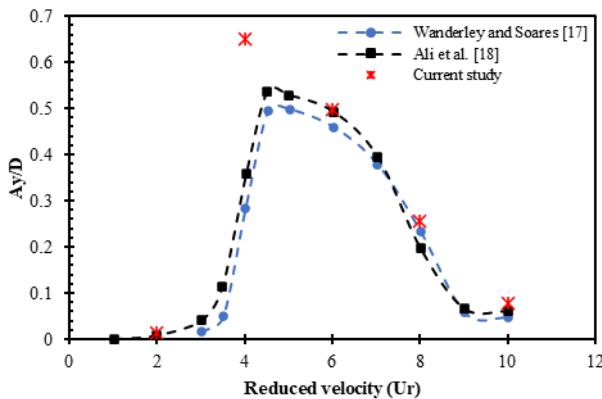


Fig. 3 The comparison between the current numerical model with the literature on the transverse normalized amplitude across a range of reduced velocities.

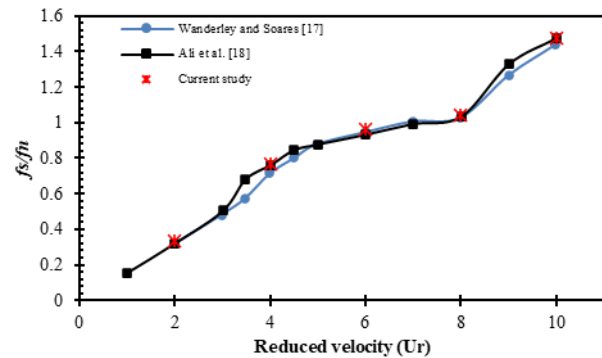


Fig. 4: The comparison between the current numerical model with the literature on the frequency ratio across a range of reduced velocities.

3. Results and discussion

To successfully evaluate the effect of the slit with various width sizes in suppressing the flow-induced vibrations, the obtained findings consisting of the normalized oscillation amplitude, lift coefficient, drag coefficient, and frequency over transverse oscillations are analyzed over an extended, fully periodic and stationary data record. The behavior of the cylinder varies depending on the selected reduced velocity, which dictates the equation of the system parameters, such as the spring constant and natural frequency. The mass ratio and damping coefficient are fixed through the reduced velocities of 2, 4, 6, 8, and 10.

3.1 Oscillation amplitude

After initiation time the cylinder starts to oscillates transversally following a sinusoidal wave form and eventually stabilizes with a fixed oscillating amplitude. This amplitude indicates the vibrating oscillating that the slits tend to subdue. The normalized amplitude-to-diameter ratio is recorded across a range of reduced velocities for a solid, 10% slitted, and 20% slitted cylinders as illustrated in Figure 5. At very low reduced velocities, the amplitude ratio and the change between cylinders are entirely insignificant. Unlike at a reduced velocity of 4 where the highest normalized transverse displacement of the cylinder occurs with a value of 0.65, 0.55, and 0.4 for the solid, 10% slitted, and 20% slitted cylinders, respectively. The displacement is reduced by 15.4% when using a slit S/D of 10% and by 38.8% when using a slit S/D of 20% at the reduced velocity of 4. The 20% slitted cylinder significantly reduces the cylinder displacement at reduced velocities of 4 and 6, where the stiffness of the spring is high. At a reduced velocity of 8 and 10, the cylinder’s displacement is subdued by 86.2% and 74.2% compared to the solid cylinder. On the other hand, with substandard performance of reducing oscillations, the 10% slitted at reduced velocities of 6, 8 and 10, the slit suppresses the motion by 7.2%, 34.9% and 15%, respectively. The main take of the comparison between integrating a slit and not is that the slitted cylinder is successful in suppressing the fluctuating amplitude of the dynamic flow on the bluff body. In addition, the effect of the 20% slit width to diameter ratio is much more significant than the 10%.

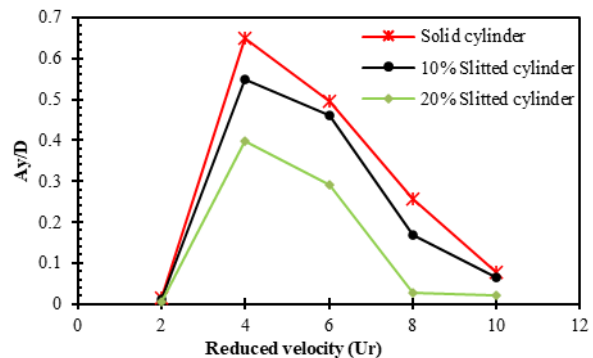


Fig. 5: The normalized oscillation amplitude of different cylinders across a range of reduced velocity.

3.2 Lift coefficient

One of the most crucial parameters in assessing the performance of the slit with various slit widths is evaluating the root mean square value of the lift coefficient (C_L). A higher C_L indicates more vital forces acting on the cylinder. The C_L is averaged all over the surface of the cylinder at a

range of reduced velocities. As demonstrated in Figure 6, the C_L is only significant at the reduced velocity of 2 till 6 where the peak is obtained at 4. Surprisingly, the effect of a 10% slit is negligible on the C_L , with a value of 1.17 at the peak when compared to the solid cylinder with a C_L of 1.2. The significant reduction of the C_L is noticed at a 20% slitted cylinder with a value of 0.8 at a reduced velocity of 4. Furthermore, at a low reduced velocity that indicates a stiff spring constant, the C_L is 0.26, and the resulting reduction is 11.8% and 72.19% for 10% slitted and 20% slitted cylinders, respectively. The parallel slit acts as a passive control method for the system by allowing the flow to pass through the cylinder and increasing the downstream pressure, stabilizing the cylinder's downstream flow and leading to a decrease in C_L . As the ratio of the width of the slit increases, such behavior is enhanced and the C_L is diminished.

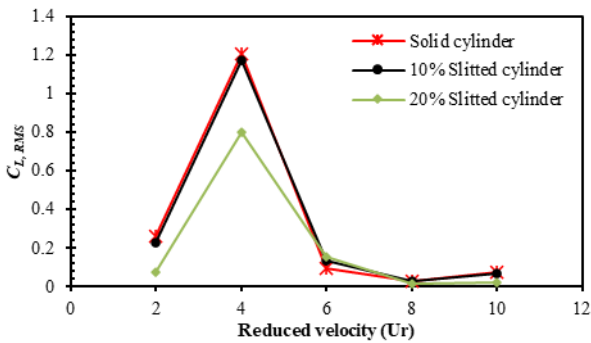


Fig. 6 The root mean square value of the lift coefficient of different cylinders across a range of reduced velocity.

3.3 Drag coefficient

The periodic average drag coefficient (C_D) shows different behavior over various reduced velocities for different slit widths. As the parallel slit is incorporated into the cylinder, the pressure distribution around the cylinder starts to change, greatly affecting the drag forces. A significant difference was found between the 20% and 10% slitted cylinders with the solid cylinder at a reduced velocity of 6, as shown in Figure 7. At $U_r = 6$, the drag is lowered by 19.57% and 4.82% when using a slit of 20% and 10% S/D, respectively. However, at $U_r = 8$, the performance of the 20% slitted cylinder is similar to that of a 10% cylinder decreasing the average C_D from 1.35 to 1.2554. Surprisingly, the 10% slitted cylinder has no effect on the C_D at a reduced velocity of 4, which is similar to the C_D case. In these ranges, the parallel slit effectively controls the flow and its corresponding forces, such as drag. Nonetheless, the analysis did not exhibit any substantial differences in behavior of the slit on the cylinder at the reduced velocities of 2 and 10. Overall, these results suggest that the reduction of drag is due to the increased

pressure caused by the fluid induced through the slit acting as a self-injecting jet downstream of the cylinder.

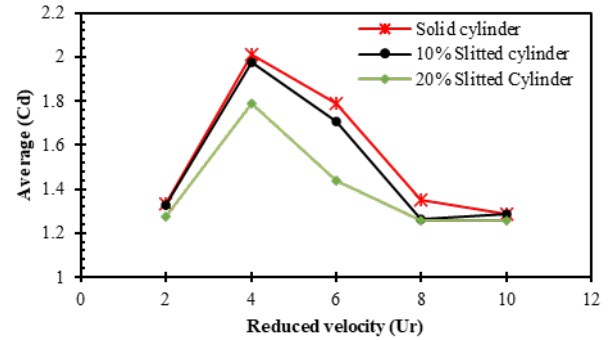


Fig. 7: The average drag coefficient of different cylinders across a range of reduced velocities.

3.4 Transverse oscillations frequency

In this section, the frequency of each oscillating cylinder is recorded to identify the lock-in phenomena, that is coincidence between natural shedding and the induced oscillation frequencies. The transverse oscillation frequency is normalized with the natural frequency at different reduced velocities. According to Figure 7, the range extending from 6 to 8 reduced velocities indicates the lock-in phenomena with a red dashed line for the solid, 10% slitted, and 20% slitted cylinders. It is also worth noting that at a reduced velocity of 8, the 10% slitted cylinder generated a two-frequency wave. The frequency of the inner wave is implemented in the Figure 8 below.

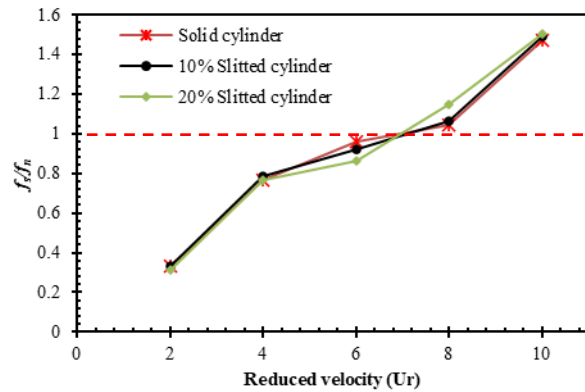


Fig. 8: The normalized transverse oscillations frequency of different cylinders across a range of reduced velocity.

Figure 9 demonstrates the vortex shedding patterns of each cylinder at reduced velocities of 4 and 6. The effect of the 10% slitted cylinder at suppressing the vortices is negligible at both reduced velocities. Because the slit does not allow sufficient flow through the cylinder to the downstream region, its ability to eradicate vibrations is limited. The pattern of vortex shedding At a reduced velocity of 4, a '2S' pattern is observed, indicating intense vibrations which correspond to higher oscillation amplitude, as shown earlier. Nonetheless, weaker vortices are generated at reduced velocities of 6. The 20% slitted cylinder

successfully diminishes the vortices into smaller bits with weaker effects.

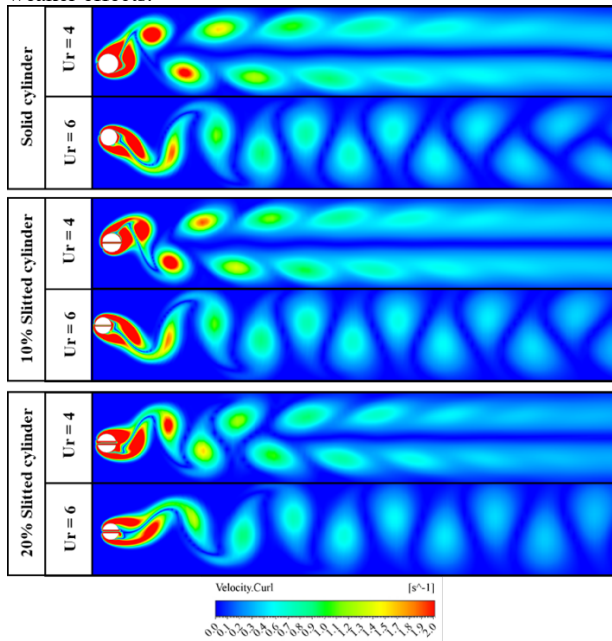


Fig. 9 Vortices contours for several types of cylinders at the reduced velocities of 4 and 6.

4. Conclusion

This work investigates the potential of incorporating parallel slits of different widths (10% and 20%) on the reduction of Flow Induced Vibrations (FIVs) on elastically mounted cylinder. The cylinder is confined to oscillate in the transverse direction only, i.e. single degree of freedom. This passive control method has the potential to efficiently eliminate induced oscillations and vibrations that are responsible for the structural damage. The effect of various parameters such as the width to diameter ratio (W/D) and the reduced velocity (U_r) to suppress the oscillating motion of the cylinder is analyzed using normalized oscillation amplitude, root mean square value of lift coefficient, mean drag coefficient, transverse oscillations frequency and vortex shedding patterns. The reported finding can be summarized as follow:

- The highest oscillation amplitude is achievable at a reduced velocity of 4 where the vortex shedding patterns indicates a ‘2S’ pattern in which the specific pattern corresponds to higher oscillation amplitude.
- The effect of a 10% slit is negligible on the lift coefficient, unlike the 20% slitted cylinder with significant reduction of the lift coefficient from 1.2 to 0.8 at a reduced velocity of 4.
- At $U_r = 6$, the drag is reduced by 19.57% and 4.82% when using slit ratios of 20% and 10%, respectively. However, at $U_r = 8$, the performance of the 20% slitted cylinder is similar to that of a 10 % cylinder, decreasing the average drag coefficient from 1.35 to 1.2554.
- Overall, the results suggest that the reduction of drag and lift forces is superior when implementing a wider slit due to the increased back pressure caused by the fluid induced through the slit acting as a downstream self-injecting jet.
- The range extending from 6 to 8 reduced velocities indicates the synchronization phenomena responsible for the oscillating cylinder displacement.

Nomenclature

CFD	Computational fluid dynamics
CFL	Courant–Friedrichs–Lewy
D	Diameter of the cylinder, m
FIV	Flow Induced Vibration
P	Pressure, Pa
PIV	Particle Image Velocimetry
RMS	Root Mean Square
S	Slit width, m
UDF	User Defined Function
URANS	Unsteady Reynolds Averaged-Navier-Stokes
U	Velocity
VIV	Vortex Induced Vibrations
k	Spring constant, N/m
l	Length, m
m	Virtual mass of the system
Δm	Added mass
y	Displacement in the y-direction, m
\dot{y}	Velocity in the y-direction, m/s
\ddot{y}	Acceleration in the y-direction, m ² /s

Greek Symbols

ν	Kinematic viscosity, Pa.s
ρ	Mass density, kg/m ³
ω	Angular frequency
f	frequency
ζ	Damping ratio

Subscripts

D	Drag
$i \ \& \ j$	Indices
L	Lift
n	Natural
r	Reduced
∞	Stream

Exponents

*	Ratio
---	-------

Non-dimensional Numbers

C	Coefficient
c	Damping coefficient
Re	Reynolds number
St	Strouhal number
Y	Non-dimensional displacement in y-direction
\dot{Y}	Non-dimensional velocity in y-direction
\ddot{Y}	Non-dimensional acceleration in y-direction

Acknowledgments

The authors would like to acknowledge Khalifa University (KU) for providing the computational resources to complete this project.

References

- [1] H. H. Khan, Md. Islam, Y. Y. Fatt, I. Janajreh, and M. M. Alam, “Effect of three tandem cylinder diameter difference on flow-induced vibrations and heat transfer,” *Int. J. Mech. Sci.*, p. 107764, Sep. 2022, doi: 10.1016/J.IJMECS.2022.107764.
- [2] V. Oruç, “Strategies for the applications of flow control downstream of a bluff body,” *Flow Meas. Instrum.*, vol. 53, pp. 204–214, Mar. 2017, doi: 10.1016/J.FLOWMEASINST.2016.08.008.
- [3] S. Kim, M. Mahbub Alam, and D. Kumar Maiti, “Wake

- and suppression of flow-induced vibration of a circular cylinder,” 2018, doi: 10.1016/j.oceaneng.2018.01.043.
- [4] J. F. Olsen and S. Rajagopalan, “Vortex shedding behind modified circular cylinders,” *J. Wind Eng. Ind. Aerodyn.*, vol. 86, no. 1, pp. 55–63, May 2000, doi: 10.1016/S0167-6105(00)00003-9.
- [5] D. L. Gao, W. L. Chen, H. Li, and H. Hu, “Flow around a circular cylinder with slit,” *Exp. Therm. Fluid Sci.*, vol. 82, pp. 287–301, Apr. 2017, doi: 10.1016/J.EXPTHERMFLUSCI.2016.11.025.
- [6] U. Ali and A. Brimmo, “Numerical Simulation of Laminar Flow Over a Transversely Oscillating Circular Cylinder,” *Int. J. Therm. Environ. Eng.*, vol. 19, no. 1, pp. 7–13, 2022, doi: 10.5383/ijtee.19.01.002.
- [7] H. Hassan, H. A. Abderrahmane, U. Ali, M. Islam, and I. Janajreh, “Numerical Analysis of Flow Over Slitted Cylinder and Experimental Validation Using Soap-Film Technique,” *Proc. ASME 2022 16th Int. Conf. Energy Sustain. ES 2022*, Sep. 2022, doi: 10.1115/ES2022-85827.
- [8] H. Zhang, L. Zhou, and T. K. T. Tse, “Mode-based energy transfer analysis of flow-induced vibration of two rigidly coupled tandem cylinders,” *Int. J. Mech. Sci.*, vol. 228, p. 107468, Aug. 2022, doi: 10.1016/J.IJMECSCI.2022.107468.
- [9] H. H. Khan, M. D. Islam, Y. Y. Fatt, I. Janajreh, and M. M. Alam, “Flow-induced vibration on two tandem cylinders of different diameters and spacing ratios,” *Ocean Eng.*, vol. 258, p. 111747, Aug. 2022, doi: 10.1016/J.OCEANENG.2022.111747.
- [10] C. Sonawane, P. Praharaj, A. Pandey, A. Kulkarni, K. Kotecha, and H. Panchal, “Case studies on simulations of flow-induced vibrations of a cooled circular cylinder: Incompressible flow solver for moving mesh problem,” *Case Stud. Therm. Eng.*, vol. 34, p. 102030, Jun. 2022, doi: 10.1016/J.CSITE.2022.102030.
- [11] V. T. Nguyen and H. H. Nguyen, “Detached eddy simulations of flow induced vibrations of circular cylinders at high Reynolds numbers,” *J. Fluids Struct.*, vol. 63, pp. 103–119, May 2016, doi: 10.1016/J.JFLUIDSTRUCTS.2016.02.004.
- [12] U. Ali, M. D. Islam, and I. Janajreh, “Flow over rotationally oscillating heated circular cylinder at low Reynolds number,” *Ocean Eng.*, vol. 265, p. 112515, Dec. 2022, doi: 10.1016/J.OCEANENG.2022.112515.
- [13] B. Su, S. He, M. Zhang, and J. Feng, “Experimental study on flow-induced vibration of a circular cylinder with a downstream square plate,” *Ocean Eng.*, vol. 247, p. 110768, Mar. 2022, doi: 10.1016/J.OCEANENG.2022.110768.
- [14] L. C. Hsu and C. L. Chen, “The drag and lift characteristics of flow around a circular cylinder with a slit,” *Eur. J. Mech. - B/Fluids*, vol. 82, pp. 135–155, Jul. 2020, doi: 10.1016/J.EUROMECHFLU.2020.02.009.
- [15] U. Ali, H. Hassan, I. Janajreh, H. A. Abderrahmane, and M. Islam, “Passive and active control for flow over a cylinder using a slit and validation with soap film technique,” *Eur. J. Mech. - B/Fluids*, Nov. 2022, doi: 10.1016/J.EUROMECHFLU.2022.11.003.
- [16] A. Mishra and A. De, “Suppression of vortex shedding using a slit through the circular cylinder at low Reynolds number,” *Eur. J. Mech. - B/Fluids*, vol. 89, pp. 349–366, Sep. 2021, doi: 10.1016/J.EUROMECHFLU.2021.06.009.
- [17] I. Janajreh, I. Talab, J. Macpherson, Numerical Simulation of Tower Rotor Interaction for Downwind Wind Turbine, Modeling and Simulation in Engineering, Vol. 10, ID: 860814, doi.org/10.1155/2010/860814
- [18] J. B. V. Wanderley and L. F. N. Soares, “Vortex-induced vibration on a two-dimensional circular cylinder with low Reynolds number and low mass-damping parameter,” *Ocean Eng.*, vol. 97, pp. 156–164, Mar. 2015, doi: 10.1016/J.OCEANENG.2015.01.012.
- [19] U. Ali, M. Islam, and I. Janajreh, “Heat transfer and wake-induced vibrations of heated tandem cylinders with two degrees of freedom: Effect of spacing ratio,” *Phys. Fluids*, vol. 34, no. 11, p. 113612, Nov. 2022, doi: 10.1063/5.0124772.